Biological and Medical Applications of Materials and Interfaces

Phase-dependent fluorescence quenching efficiency of MoS2 nanosheet and its applications in multiplex target biosensing

Lingyi Lan, Danke Chen, Yao Yao, Xinsheng Peng, Jian Wu, Yanbin Li, Jianfeng Ping, and Yibin Ying

ACS Appl. Mater. Interfaces, **Just Accepted Manuscript** • DOI: 10.1021/acsami.8b15677 • Publication Date (Web): 13 Nov 2018

Phase-dependent fluorescence quenching efficiency of MoS_2 nanosheet and its applications in multiplex target biosensing

Lingyi Lan[a], Danke Chen[c], Yao Yao[a], Xinsheng Peng[c], Jian Wu[a], Yanbin Li[a, d], Jianfeng Ping[a, *], Yibin Ying[a, b]

[a] School of Biosystems Engineering and Food Science, Zhejiang University, Hangzhou, Zhejiang 310058, China

[b] Zhejiang A&F University, Hangzhou, Zhejiang 311300, China

[c] State Key Laboratory of Silicon Materials, School of Materials Science and Engineering, Zhejiang University, Hangzhou, 310027, China

[d] Department of Biological and Agricultural Engineering, Center of Excellence for Poultry Science, University of Arkansas, Fayetteville, AR 72701, USA

Corresponding author: Prof. Jianfeng Ping

E-mail: jfping@zju.edu.cn

Abstract: Two-dimensional layered transition-metal dichalcogenides nanosheets have shown great potential in biosensors owing to their unique properties. Here, we exfoliated ultrathin metallic and semiconductive MoS_2 nanosheets based on a chemical exfoliation method. We compared the difference of fluorescence quenching efficiency between metallic and semiconductive MoS_2 nanosheets. We found that the fluorescence quenching efficiency of MoS_2 nanosheets is phase-dependent. The ultrathin metallic MoS_2 nanosheets with larger contents of 1T-phase structure show higher fluorescence quenching efficiency than semiconductive MoS_2 nanosheets, which can be ascribed to the higher conductivity of metallic MoS_2 nanosheets. Based on the excellent fluorescence quenching efficiency of metallic MoS_2 nanosheet and its discriminative adsorption towards single-strand DNA and double-strand DNA, a fluorescent biosensor for multiplex detection of DNA was developed. This fluorescent biosensing platform allows simultaneous fluorescence quenching of two single-strand DNA probes labeled with different fluorophores, resulting in multiplex detection of different DNA sequences in one homogeneous solution with high sensitivity.

Keywords: chemical exfoliation, MoS_2 nanosheets, 1T-phase, 2H-phase, fluorescence quenching, multiplex detection

1. Introduction

Two-dimensional (2D) layered transition-metal dichalcogenides (TMDs) nanosheets, such as MoS_2, WS_2, $MoSe_2$, and WSe_2, have aroused great attention recently in virtue of their superior physical, optical and electrochemical properties as well as their planar structure.[1] Every individual layer of bulk TMDs is formed by a sandwich structure which consists of a transition metal atomic layer between two chalcogen atomic layers and then these layers are stacked up by weak van der Waals interactions.[2] When bulk TMDs materials are thinned into nanosheets, both optical and electronic properties are enhanced,[3] which promotes their applications in the field of batteries,[4] transistors,[5] capacitors,[6] and biosensors.[7]

Up to now, numerous approaches (e.g. mechanical cleavage,[8] sonication-assisted exfoliation,[9] electrochemical exfoliation,[10] and chemical exfoliation[11]) have been utilized to prepare single- or few-layer TMDs nanosheets from bulk materials. Among these methods, chemical exfoliation has been considered as the one of most promising methods in view of its high yield of single- or few-layer TMDs nanosheets. Particularly, the organolithium-based chemical exfoliation method can produce ultrathin TMDs nanosheets with large contents of metallic 1T-phase structure (orthogonal).[12] This phase structure, recently, has been found to be more active and conductive than the common crystalline phase structure (2H-phase, trigonal prismatic) of TMDs[13] and TMDs with this phase structure have shown great potential in electrochemistry-related applications, such as supercapacitors,[14] biosensors,[15-16] and actuators.[17]

It has been reported that single- or few-layer 2D TMDs nanosheets are considered to be an ideal class of nanomaterials for fluorescent biosensors due to their excellent fluorescence quenching ability.[18] However, the reason why 2D TMDs nanosheets possess excellent fluorescence quenching ability is not clear. Furthermore, whether there is a difference between TMDs nanosheets with different phase structure has not been explored yet. Herein, we compared the fluorescence quenching ability of both metallic and semiconductive MoS_2 nanosheets and found that the metallic MoS_2 nanosheets exhibit higher fluorescence quenching efficiency towards fluorophore-labeled ssDNA. This is mainly attributed to its larger contents of 1T-phase structure than semiconductive MoS_2 nanosheets, which makes it more active and conductive and thus leading to its higher fluorescence quenching efficiency. Based on this, a metallic MoS_2-based fluorescent biosensor was proposed for multiplex detection of ssDNA in one homogeneous solution with high sensitivity.

2. Experimental

Preparation of metallic and semiconductive MoS_2 nanosheets. Ultrathin MoS_2 nanosheets were obtained from the layered bulk MoS_2 via chemical lithium-intercalation method. In brief, 0.2 g of bulk molybdenum disulfide powder was first suspended in 2.0 mL of 1.6 M *n*-Butyllithium solution. Next, it was stirred under argon atmosphere in a glove box for 48 h. Subsequently, the intercalated compound was washed with hexane for several times using vacuum filtration. For metallic MoS_2 nanosheets, the intercalated compound powder was directly dispersed in distilled water and ultrasonicated for 60 min. Then, the obtained well-dispersed suspension was centrifugated to remove the unexfoliated MoS_2, the supernatant was collected and centrifugated at 8000 rpm for 20 min. Finally, the sediment was collected and dispersed in distilled water. To get semiconductive MoS_2 nanosheets, the intercalated compound was first annealed at 300 ºC under Ar and H_2 protection for 2 h, then the annealed product was dispersed in water (100 mL) and ultrasonicated for 60 min. The centrifugation process is the same with the process for metallic MoS_2 nanosheets. The concentration of the final suspension was measured via ICP-MS.

Fluorescent DNA detection assays. In a typical DNA hybridization assay, 10 nM FAM–labeled probe 1 (P1) or 15 nM Texas red–labeled probe 2 (P2) was hybridized with different concentrations of target 1 (T1, the specific sequence of mecA gene of *Staphylococcus aureus*) or target 2 (T2, the specific sequence of eae gene of *Escherichia coli* O157:H7). After the addition of MoS_2 nanosheets, the mixture was incubated for 5 min and then the fluorescence emission spectra was measured. For T2 detection, fluorescence spectra was obtained at an excitation wavelength of 585 nm and an emission wavelength range of 605–700 nm. In a multiplex DNA hybridization assay, 3 nM FAM-labeled P1 and 10 nM Texas red-labeled P2 were mixed together in one homogenous solution. Here, different concentrations of probes were used for the optimization of the detection performance. All the measuring conditions were the same with those in the single target detection.

3. Results and discussion

Exfoliation of metallic and semiconductive MoS_2 nanosheets. The methods to obtain MoS_2 nanosheets are shown in **Figure 1**. MoS_2 bulk powder was first mixed with *n*-Butyllithium solution in hexane for 48 h to insert lithium ions into the layered structures of bulk MoS_2. The obtained Li-intercalated MoS_2 (Li_xMoS_2) compound will be exfoliated to nanosheets via ultrasonication, obtaining a dispersion of metallic MoS_2 nanosheets contains large contents of 1T-phase structure.

This was attributed to phase change from the pristine 2H-phase to 1T-phase that occurs during Li intercalation.[19] As reported, 1T-phase structure could transform to stable 2H-phase structure upon annealing, the material is predominantly in 2H-phase structure after annealing around 300 ºC.[20] Inspired by this, the obtained Li-intercalated MoS_2 (Li_xMoS_2) compound was first annealed at 300 ºC under Ar and H_2 protection for 2 h before dispersed in water, leading to the formation of semiconductive MoS_2 nanosheets after ultrasonication.

Basic characterizations of metallic and semiconductive MoS_2 nanosheets. Morphologies and chemical components of the obtained metallic and semiconductive MoS_2 nanosheets were characterized using SEM, TEM, AFM, Raman, and XPS. The SEM images demonstrate that the obtained MoS_2 nanosheets possess plane sizes ranging from hundreds of nanometers to a few micrometers **(Figure 2a, 2d**). The TEM image in **Figure 2b** shows a typical metallic ultrathin MoS_2 nanosheets. From the scanning transmission electron microscopy (STEM) image (inset in **Figure 2b**), the arrangement of Mo atoms can be observed, corresponding to 1T-phase arrangement. For semiconductive MoS_2 nanosheets (**Figure 2e**), the arrangement of Mo and S atoms can be observed, which is consistent with 2H-phase structure. AFM characterization (**Figure 2c, 2f**) illustrates that the thickness of the metallic MoS_2 nanosheets ranges from 1.6 to 4.0 nm, while that of semiconductive MoS_2 nanosheets ranges from 2.8 to 5.0 nm. Furthermore, Raman spectroscopy was carried out for characterizing atomic structural arrangement of MoS_2. As reported, 1T-phase MoS_2 has distinctive Raman peaks (J_1, J_2, E^1_g, and J_3) in addition to the in-plane mode E^1_{2g} and the out-of-plane mode A_{1g}.[22] As shown in **Figure 3a**, the bulk MoS_2 and semiconductive MoS_2 nanosheets only show two typical Raman modes (E^1_{2g} and A_{1g}), while the exfoliated metallic MoS_2 nanosheets show the presence of J_1, J_2, E^1_g, and J_3 peaks, which identify the 1T-phase structure.[17, 20] In addition, XPS was carried out to quantify the fraction of each phase. The peaks of Mo^{4+} $3d_{5/2}$ and Mo^{4+} $3d_{3/2}$ components of 2H-phase MoS_2 (green curve) are around 229.1 eV and 232.2 eV, respectively, while that of 1T-phase MoS_2 (red curve) are around 228.1 eV and 231.2 eV, respectively. **Figure 3b** shows the high resolution spectra of Mo 3d bonding modes of metallic MoS_2 nanosheets. On the basis of the deconvolutions, it can be calculated that the 1T-phase content of the metallic nanosheets is around 70%. However, the 1T-phase content of the semiconductive MoS_2 nanosheets decreases sharply while the contribution from the 2H-phase increases (**Figure 3c**), where the spectrum is quite similar to the bulk 2H-phase MoS_2 (**Figure 3d**), which further confirm the occurrence of phase

change during the annealing process. To further confirm the phase difference between metallic and semiconductive MoS_2 nanosheets, optical absorption measurement is carried out, as illustrated in **Figure 4a**. For semiconductive MoS_2 nanosheets, obvious absorption peak can be shown in the UV−vis spectrum (red line), which is due to its large contents of 2H-phase structure. On the contrary, no distinct absorption peak can be observed for that of metallic MoS_2 nanosheets (black line). As reported, metallic MoS_2 nanosheets with larger contents of 1T-phase structure is more active and conductive than semiconductive MoS_2 nanosheets. To figure out this, we measured the conductivity of the two films obtained by vacuum filtration. The conductivity of the films was measured by a commercialized four-point probe conductivity tester. As illustrated in **Figure 4b,** the conductivity of semiconductive MoS_2 nanosheets is only 9.7×10^{-4} S/cm, while that of metallic MoS_2 nanosheets is 69.2 S/cm, which is nearly 7×10^4 times than semiconductive MoS_2 nanosheets. Meanwhile, the color of semiconductive MoS_2 nanosheets solution is dark grey (**Figure 4c**), while that of metallic MoS_2 nanosheets is black (**Figure 4d**). The color difference is more obvious when the solution is filtrated into films. This results confirm that metallic MoS_2 nanosheets is more conductive than the semiconductive MoS_2 nanosheets, which may broaden its applications in biosensing fields.

Comparison of fluorescence quenching efficiency of metallic and semiconductive MoS_2 nanosheets. DNA detection has always been essential in various areas such as disease genetics,[21] life science, and food safety.[22] Biosensors with different signal-transducing mechanisms (e.g. optical, electrochemical, and piezoelectric) are widely studied for DNA detection.[23-25] Among them, fluorescent biosensors based on the fluorescence quenching ability of nanomaterials (e.g. graphene oxide (GO),[26] MnO_2 nanosheets,[27] carbon nanotubes,[28] gold nanoparticles,[29] and graphene oxide quantum dots[30]) have been extensively employed owing to the merits of high sensitivity, simple operation, rapid hybridization kinetics, and easy automation.[31] In particular, single- or few-layer 2D TMDs nanosheets recently have proved to be an ideal class of nanomaterials due to their excellent fluorescence quenching ability[32] and the discriminative adsorption towards single-strand DNA (ssDNA) and double-strand DNA (dsDNA). Based on this, we suppose that the metallic MoS_2 nanosheets with high conductivity may be a good choice as fluorescent quenchers in biosensing platform for the detection of ssDNA.

To compare the fluorescence quenching efficiency between metallic MoS_2 nanosheets and semiconductive MoS_2 nanosheets, fluorescence quenching for fluorophore-labeled ssDNA

experiments were carried out in the presence of metallic and semiconductive MoS_2 nanosheets with the same concentration. As shown in **Figure 4e**, it can be observed that under same concentration (4.65 μg mL^{-1}), the fluorescence quenching efficiency of semiconductive MoS_2 nanosheets is only around 2%, while for metallic MoS_2 nanosheets, the quenching efficiency is almost 98.5%. To obtain similar fluorescence quenching efficiency with metallic MoS_2 nanosheets, 500 μg mL^{-1} of semiconductive MoS_2 nanosheets is needed, which is over 100-fold than that of metallic MoS_2 nanosheets (**Figure 4f**). To determine the quenching constants of metallic and semiconductive MoS_2 nanosheets, the change of fluorescence intensity of FAM-labeled ssDNA was measured under different concentrations of MoS_2 nanosheets. The fluorescence quenching ability of ultrathin metallic and semiconductive MoS_2 nanosheets is illustrated in **Figure 5a-b** and **Figure S1a-b** (Supporting Information), respectively. As reported, fluorescence quenching can be divided into static quenching and dynamic quenching. The dynamic quenching follows Stern-Volmer's equation[33], while the static quenching follows the Lineweaver-Burk equation.[34] As illustrated in **Figure S1c-d** (Supporting Information), the relationship between F_0/F and MoS_2 concentration doesn't correspond to Stern-Volmer's equation, while that between (F_0-F) and MoS_2 concentration follows the Lineweaver-Burk equation. Thus, it can be proved that the fluorescence quenching of MoS_2 nanosheets to FAM-labeled ssDNA is static quenching. According to the Lineweaver-Burk equation, the static quenching constants of metallic and semiconductive MoS_2 nanosheets were calculated to be 15.32 and 0.012 μg mL^{-1}, respectively. These results indicate higher fluorescence quenching efficiency of metallic MoS_2 nanosheets than semiconductive MoS_2 nanosheets in this fluorescent bioassay.

To figure out the reason why metallic MoS_2 nanosheets exhibited higher fluorescence quenching efficiency than semiconductive MoS_2 nanosheets, it is necessary to explore the fluorescence quenching mechanism between MoS_2 nanosheets and fluorophore-labeled ssDNA. As reported, the fluorescence quenching mechanism between 2D nanosheets and fluorophore-labeled ssDNA mainly have two types, that is, Förster resonance energy transfer (FRET)[26] and electron transfer (ET).[35] The FRET-based fluorescence quenching is attributed to the overlap between the emission spectrum of donor and the absorption spectrum of acceptor. As shown in **Figure S2** (Supporting Information), the overlap between emission spectrum of FAM-labeled ssDNA and absorption spectrum of MoS_2 nanosheets suggested the occurrence of FRET. Furthermore, as

reported, the fluorophore-labeled ssDNA can be absorbed onto the surface of MoS_2 nanosheets due to physical absorption,[36] which resulted in a close contact of the fluorophore with MoS_2 nanosheets to produce a remarkable electronic communication between them. The electronic communication led to the fluorescence quenching of fluorophore. Therefore, it comes to the conclusion that the fluorescence quenching between MoS_2 nanosheets and fluorophore-labeled ssDNA was attributed to both FRET and ET mechanism. Considering the fact that ssDNA can be absorbed onto both surface of metallic and semiconductive MoS_2 nanosheets, the Förster distance of them shows little difference, so the fluorescence quenching difference caused by FRET could be excluded. Therefore, the fluorescence quenching difference can be mainly ascribed to the ET mechanism. Noting that the zeta potential values of the two kinds of nanosheet also show little difference (**Table S1** in Supporting Information), so we ascribe this phenomenon to the different conductivity of the metallic and semiconductive MoS_2 nanosheets. The obtained metallic MoS_2 nanosheets is more conductive than the semiconductive MoS_2 nanosheets owing to the higher 1T-phase contents,[37] which means faster electron transfer. In this way, when quenching the fluorescence of fluorophore-labeled ssDNA, the electrons on the surface of metallic MoS_2 nanosheets would transfer faster than the semiconductive ones, which facilitate electron transfer kinetics during the fluorescence quenching process, and thus enhance the fluorescence quenching efficiency.

Optimization of experimental conditions. The results shown above demonstrated that metallic MoS_2 nanosheets possess higher conductivity as well as higher fluorescence quenching efficiency than the semiconductive ones. Therefore, it is a better choice as fluorescent quenchers in biosensing platform for ssDNA determination. The DNA sequences used in this experiment are listed in **Table S2** (Supporting Information). To evaluate the fluorescence quenching ability of the ultrathin metallic MoS_2 nanosheets, 10 nM FAM-labeled P1 was mixed with different concentrations of MoS_2 nanosheets ranging from 0 to 6.51 μg mL^{-1}. It can be observed that the quenching of the probe fluorescence is concentration-dependent (**Figure 5a and b**). Moreover, the quenching kinetics is extremely fast, nearly 98.5% of the P1 fluorescence is quenched within 5 min after the addition of 4.65 μg mL^{-1} of MoS_2 nanosheets (**Figure 5a**). Next, the recovery of the P1 fluorescence upon the addition of T1 in the presence of different concentrations of MoS_2 nanosheets was examined (**Figure 5c**). Based on the curve in **Figure 5d**, it can be calculated that the recovery efficiency is nearly 99% under the 4.65 μg mL^{-1} of MoS_2 nanosheets. Moreover, when the concentration of MoS_2

is higher than 4.65 μg mL^{-1}, the recovery efficiency shows no obvious increase. Therefore, 4.65 μg mL^{-1} of MoS_2 nanosheets was chosen as the optimal concentration for the fluorescence quenching of 10 nM FAM-labeled P1.

Although metallic MoS_2 nanosheets exhibit higher fluorescence quenching efficiency than semiconductive one, it is less stable due to its chemical reactivity. When exposed to air or in aqueous media, Mo^{4+} can easily be oxidized into Mo^{6+}.[13, 20] Therefore, it is crucial to study the stability of metallic MoS_2 nanosheets in this fluorescence biosensing strategy. From **Figure 6a**, it can be observed that the 1T-phase content of metallic MoS_2 nanosheets shows a slight decrease (from ~70% to ~65%) as time goes on (from day 1 to day 7), which may attribute to the formation of oxidized products of molybdenum (violet curve in **Figure 6b**). In order to figure out whether this change would influence its analytical performance, the fluorescence quenching efficiency of metallic MoS_2 nanosheets with different storage time was evaluated. As illustrated in **Figure 6c**, though a slight decrease is observed, the fluorescence quenching efficiency of metallic MoS_2 nanosheets remains high (~98%), indicating that the formation of oxidized products produce negligible effect on the fluorescence quenching ability of metallic MoS_2 nanosheets.

Detection feasibility. The working mechanism of multiplex analysis of two DNA based on ultrathin metallic MoS_2 nanosheets is illustrated in **Figure S3** (Supporting Information). When incubated the fluorophore-labeled probe with MoS_2 nanosheets, the probe would be absorbed onto the surface of MoS_2 nanosheets via physical absorption. In this way, the fluorescence of the probe is quenched by MoS_2 nanosheets. In the presence of target, the probe would hybridize with its target and form dsDNA. The rigid structure of dsDNA would weaken its interaction with MoS_2 nanosheets, resulting in its release from the surface of MoS_2 nanosheets and consequently the recovery of the fluorescence signal.

To investigate the affinity of MoS_2 nanosheets towards ssDNA and dsDNA, fluorescence spectra of FAM-labeled P1 under various experimental conditions was measured. As shown in **Figure S4** (Supporting Information), P1 displays a strong fluorescence emission (black curve in **Figure S4b**). Upon the addition of MoS_2 nanosheets at optimal concentration (4.65 μg mL^{-1}), the fluorescence intensity reduces immediately (green curve in **Figure S4b**), almost 2% of the original value, indicating the rapid quenching of FAM-labeled P1. When mixed P1 with its complementary DNA (T1) of an equal amount, dsDNA (P1T1 duplex) formed. It can be observed that the

fluorescence of P1T1 duplex is largely retained when incubated with MoS_2 nanosheets (blue curve in **Figure S4b**), nearly 75–fold higher than that of P1 in the presence of MoS_2 nanosheets. These results demonstrate that interaction between dsDNA and MoS_2 nanosheets is much weaker than that between ssDNA and MoS_2 nanosheets.

Analytical performance of single DNA detection. Based on the aforementioned results, the ultrathin metallic MoS_2 nanosheet can serve as an ideal fluorescence quencher for the determination of DNA. First, 10 nM FAM-labeled P1 was mixed with a series of concentrations of T1 (0–75 nM) for 30 min. Next, metallic MoS_2 nanosheets with the optimized concentration was added to the mixture, which served as fluorescence quencher. As the concentration of T1 increases, the fluorescence intensity also increases accordingly (**Figure 7a**). From the calibration curve (**Figure 7b**), this biosensor shows a linear range from 0–4 nM, with a detection limit (LOD) of 120 pM (LOD=3σ/S, σ is the standard deviation of the background signal and S represents the slope of the calibration curve). Similar results are also observed when 15 nM Texas red-labeled P2 is hybridized with different concentrations of T2 (0–75 nM) at room temperature for 30 min (**Figure 7c**). The linear range is from 0 to 4 nM, with a LOD of 330 pM (**Figure 7d**). The analytical performance of semiconductive MoS_2 nanosheets for DNA detection was also tested, as shown in **Figure S5** (Supporting Information). Results demonstrated that the LOD of semiconductive MoS_2 nanosheets-based fluorescent sensor is 0.65 nM for T1 and 0.97 nM for T2. To compare the analytical performance of this MoS_2-based biosensing assay with other TMDs based DNA biosensor, a comparative study with other literature was shown in **Table S3** (Supporting Information).

Selectivity test. To evaluate the specificity of the proposed fluorescent biosensor towards different DNA sequences, the target DNA (T1 and T2), single-base mismatched DNA (SM1, SM2 for P1, P2, respectively), two-base mismatched DNA (TM1, TM2 for P1, P2, respectively), and random DNA (R1, R2 for P1, P2, respectively) were investigated. The results prove that this MoS_2-based fluorescent biosensor exhibits high selectivity towards the target DNA (**Figure S6**, Supporting Information).

Multiplex detection. As is known to all, multiplex DNA detection is vital in medical diagnostics, gene therapy, environmental monitoring, and food safety. Therefore, we employed this biosensing strategy for simultaneous detection of different DNA (T1, the specific sequence of mecA gene of *Staphylococcus aureus* and T2, the specific sequence of eae gene of *Escherichia coli* O157:H7) with

different fluorophore-labeled probes (P1, P2). These probes labeled with various fluorophores would only hybridize with its specific target DNA and emit at the corresponding wavelengths as shown in **Figure 8**. In the presence of T1 (3 nM) only, the specific emission of P1 at 521 nm is induced (**Figure 8a**). While the presence of T2 (10 nM) only induces the emission of P2 at 615 nm (**Figure 8b**). When P1 and P2 are mixed with T1 and T2 in a homogeneous solution, the induced emission of both P1 and P2 are observed with two different emission peaks (**Figure 8c**). However, in the absence of T1 and T2, no emission peaks are observed (**Figure 8d**). These results demonstrate the feasibility of MoS_2 nanosheets-based fluorescent biosensor towards different DNA sequences.

4. Conclusions

In conclusion, we demonstrated that the ultrathin metallic MoS_2 nanosheets with larger contents exhibit higher fluorescence quenching efficiency than semiconductive MoS_2 nanosheets owing to its higher conductivity. Furthermore, On the basis of these findings, a rapid and sensitive fluorescent biosensing strategy for multiplex DNA detection was established. Therefore, we anticipate that this proposed ultrathin metallic MoS_2-based fluorescent biosensor would pave a way for the development of rapid, simple, and robust multiplex detection method of biological molecules and hold great potential in the field of medical diagnostics, gene therapy as well as food safety.

Supporting information

Methods and instruments; zeta potential of the metallic and semiconductive MoS_2 nanosheets; specific sequence of DNA used in this work; comparison of different 2D TMDs-based fluorescent DNA sensors; fluorescence quenching ability of semiconductive MoS_2 nanosheets; emission spectrum of FAM-labeled ssDNA and absorption spectrum of metallic and semiconductive MoS_2 nanosheets; working mechanism of multiplex analysis of two DNA; fluorescence response of samples with and without the addition of T1 in the presence of MoS_2 nanosheets; detection performance of semiconductive MoS_2 nanosheets; selectivity of the MoS_2-based fluorescent biosensor.

Author information

Corresponding Author

*E-mail: jfping@zju.edu.cn.

ORCID

Jianfeng Ping: 0000-0002-0579-9830

Notes

The authors declare no competing financial interest.

Acknowledgments

This work was supported by the National Natural Science Foundation of China (31571922).

References

(1) Zhang, H. Ultrathin Two-Dimensional Nanomaterials. *ACS Nano* **2015,** *9* (10), 9451-9469.

(2) Tan, C.; Zhang, H. Two-Dimensional Transition Metal Dichalcogenide Nanosheet-Based Composites. *Chem. Soc. Rev.* **2015,** *44* (9), 2713-2731.

(3) Chhowalla, M.; Shin, H. S.; Eda, G.; Li, L.-J.; Loh, K. P.; Zhang, H. The Chemistry of Two-Dimensional Layered Transition Metal Dichalcogenide Nanosheets. *Nat. Chem.* **2013,** *5* (4), 263-275.

(4) Voiry, D.; Yamaguchi, H.; Li, J.; Silva, R.; Alves, D. C. B.; Fujita, T.; Chen, M.; Asefa, T.; Shenoy, V. B.; Eda, G.; Chhowalla, M. Enhanced Catalytic Activity in Strained Chemically Exfoliated WS_2 Nanosheets for Hydrogen Evolution. *Nat. Mater.* **2013,** *12* (9), 850-855.

(5) Sarkar, D.; Xie, X.; Kang, J.; Zhang, H.; Liu, W.; Navarrete, J.; Moskovits, M.; Banerjee, K. Functionalization of Transition Metal Dichalcogenides with Metallic Nanoparticles: Implications for Doping and Gas-Sensing. *Nano Lett.* **2015,** *15* (5), 2852-2862.

(6) Wang, H.; Feng, H.; Li, J. Graphene and Graphene-Like Layered Transition Metal Dichalcogenides in Energy Conversion and Storage. *Small* **2014,** *10* (11), 2165-2181.

(7) Pumera, M.; Loo, A. H. Layered Transition-Metal Dichalcogenides (MoS_2 and WS_2) for Sensing and Biosensing. *Trends Anal. Chem.* **2014,** *61*, 49-53.

(8) Novoselov, K. S.; Jiang, D.; Schedin, F.; Booth, T. J.; Khotkevich, V. V.; Morozov, S. V.; Geim, A. K. Two-Dimensional Atomic Crystals. *Proc. Natl. Acad. Sci. U. S. A.* **2005,** *102* (30), 10451-10453.

(9) Smith, R. J.; King, P. J.; Lotya, M.; Wirtz, C.; Khan, U.; De, S.; O' Neill, A.; Duesberg, G. S.; Grunlan, J. C.; Moriarty, G.; Chen, J.; Wang, J.; Minett, A. I.; Nicolosi, V.; Coleman, J. N. Large-Scale Exfoliation of Inorganic Layered Compounds in Aqueous Surfactant Solutions. *Adv. Mater.* **2011,** *23* (34), 3944-3948.

(10) Zeng, Z.; Yin, Z.; Huang, X.; Li, H.; He, Q.; Lu, G.; Boey, F.; Zhang, H. Single-Layer Semiconducting Nanosheets: High-Yield Preparation and Device Fabrication. *Angew. Chem. Int.*

Ed. **2011,** *50* (47), 11093-11097.

(11) Zheng, J.; Zhang, H.; Dong, S.; Liu, Y.; Nai, C. T.; Shin, H. S.; Jeong, H. Y.; Liu, B.; Loh, K. P. High Yield Exfoliation of Two-Dimensional Chalcogenides Using Sodium Naphthalenide. *Nat. Commun.* **2014,** *5,* 2995.

(12) Ambrosi, A.; Sofer, Z.; Pumera, M. 2H -> 1T Phase Transition and Hydrogen Evolution Activity of MoS_2, $MoSe_2$, WS_2 and WSe_2 Strongly Depends on the MX_2 Composition. *Chem. Commun.* **2015,** *51* (40), 8450-8453.

(13) Kurapati, R.; Muzi, L.; de Garibay, A. P. R.; Russier, J.; Voiry, D.; Vacchi, I. A.; Chhowalla, M.; Bianco, A. Enzymatic Biodegradability of Pristine and Functionalized Transition Metal Dichalcogenide MoS_2 Nanosheets. *Adv. Funct. Mater.* **2017,** *27* (7), 1605176.

(14) Lei, Z.; Zhan, J.; Tang, L.; Zhang, Y.; Wang, Y. Recent Development of Metallic (1T) Phase of Molybdenum Disulfide for Energy Conversion and Storage. *Adv. Energy Mater.* **2018,** *8* (19), 1703482.

(15) Toh, R. J.; Mayorga-Martinez, C. C.; Sofer, Z.; Pumera, M. 1T-Phase WS_2 Protein-Based Biosensor. *Adv. Funct. Mater.* **2017,** *27* (5), 1604923.

(16) Nasir, M. Z. M.; Mayorga-Martinez, C. C.; Sofer, Z.; Pumera, M. Two-Dimensional 1T-Phase Transition Metal Dichalcogenides as Nanocarriers to Enhance and Stabilize Enzyme Activity for Electrochemical Pesticide Detection. *ACS Nano* **2017,** *11* (6), 5774-5784.

(17) Acerce, M.; Akdoğan, E. K.; Chhowalla, M. Metallic Molybdenum Disulfide Nanosheet-Based Electrochemical Actuators. *Nature* **2017**, 23668.

(18) Zhang, Y.; Zheng, B.; Zhu, C. F.; Zhang, X.; Tan, C. L.; Li, H.; Chen, B.; Yang, J.; Chen, J. Z.; Huang, Y.; Wang, L. H.; Zhang, H. Single-Layer Transition Metal Dichalcogenide Nanosheet based Nanosensors for Rapid, Sensitive, and Multiplexed Detection of DNA. *Adv. Mater.* **2015,** *27* (5), 935-939.

(19) Eda, G.; Yamaguchi, H.; Voiry, D.; Fujita, T.; Chen, M.; Chhowalla, M. Photoluminescence from Chemically Exfoliated MoS_2. *Nano Lett.* **2012,** *12* (1), 526-526.

(20) Voiry, D.; Salehi, M.; Silva, R.; Fujita, T.; Chen, M.; Asefa, T.; Shenoy, V. B.; Eda, G.; Chhowalla, M. Conducting MoS_2 Nanosheets as Catalysts for Hydrogen Evolution Reaction. *Nano Lett.* **2013,** *13* (12), 6222-6227.

(21) McCarthy, J. J.; Hilfiker, R. The Use of Single-Nucleotide Polymorphism Maps in

Pharmacogenomics. *Nat. Biotechnol.* **2000,** *18* (5), 505-508.

(22) Tabrizi, M. A.; Shamsipur, M. A Label-Free Electrochemical DNA Biosensor Based on Covalent Immobilization of Salmonella DNA Sequences on the Nanoporous Glassy Carbon Electrode. *Biosens. Bioelectron.* **2015,** *69*, 100-105.

(23) Wu, S.; Zeng, Z.; He, Q.; Wang, Z.; Wang, S. J.; Du, Y.; Yin, Z.; Sun, X.; Chen, W.; Zhang, H. Electrochemically Reduced Single-Layer MoS_2 Nanosheets: Characterization, Properties, and Sensing Applications. *Small* **2012,** *8* (14), 2264-2270.

(24) Li, B. L.; Zou, H. L.; Lu, L.; Yang, Y.; Lei, J. L.; Luo, H. Q.; Li, N. B. Size-Dependent Optical Absorption of Layered MoS_2 and DNA Oligonucleotides Induced Dispersion Behavior for Label-Free Detection of Single-Nucleotide Polymorphism. *Adv. Funct. Mater.* **2015,** *25* (23), 3541-3550.

(25) Lan, L.; Yao, Y.; Ping, J.; Ying, Y. Recent Progress in Nanomaterial-Based Optical Aptamer Assay for the Detection of Food Chemical Contaminants. *ACS Appl. Mater. Interfaces* **2017,** *9* (28), 23287-23301.

(26) Lu, C.-H.; Yang, H.-H.; Zhu, C.-L.; Chen, X.; Chen, G.-N. A Graphene Platform for Sensing Biomolecules. *Angew. Chem. Int. Ed.* **2009,** *48* (26), 4785-4787.

(27) Qu, F.; Pei, H.; Kong, R.; Zhu, S.; Xia, L. Novel Turn-on Fluorescent Detection of Alkaline Phosphatase Based on Green Synthesized Carbon Dots and MnO_2 Nanosheets. *Talanta* **2017,** *165*, 136-142.

(28) Satishkumar, B. C.; Brown, L. O.; Gao, Y.; Wang, C.-C.; Wang, H.-L.; Doorn, S. K. Reversible Fluorescence Quenching in Carbon Nanotubes for Biomolecular Sensing. *Nat. Nanotechnol.* **2007,** *2* (9), 560-564.

(29) Pei, H.; Zheng, Y.; Kong, R.; Xia, L.; Qu, F. Niche Nanoparticle-Based FRET Assay for Bleomycin Detection Via DNA Scission. *Biosens. Bioelectron.* **2016,** *85*, 76-82.

(30) Pei, H.; Zhu, S.; Yang, M.; Kong, R.; Zheng, Y.; Qu, F. Graphene Oxide Quantum Dots@Silver Core-Shell Nanocrystals as Turn-on Fluorescent Nanoprobe for Ultrasensitive Detection of Prostate Specific Antigen. *Biosens. Bioelectron.* **2015,** *74*, 909-914.

(31) Lan, L.; Yao, Y.; Ping, J.; Ying, Y. Recent Advances in Nanomaterial-Based Biosensors for Antibiotics Detection. *Biosens. Bioelectron.* **2017,** *91*, 504-514.

(32) Kong, R.-M.; Ding, L.; Wang, Z.; You, J.; Qu, F. A Novel Aptamer-Functionalized MoS_2 Nanosheet Fluorescent Biosensor for Sensitive Detection of Prostate Specific Antigen. *Anal.*

Bioanal. Chem. **2015,** *407* (2), 369-377.

(33) Sauer, K.; Scheer, H.; Sauer, P. Forster Transfer Calculations Based on Crystal-Structure Data from Agmenellum-Quadruplicatum C-Phycocyanin. *Photochem. Photobiol.* **1987,** *46* (3), 427-440.

(34) Murphy, C. B.; Zhang, Y.; Troxler, T.; Ferry, V.; Martin, J. J.; Jones, W. E. Probing Forster and Dexter Energy-Transfer Mechanisms in Fluorescent Conjugated Polymer Chemosensors. *J. Phys. Chem. B* **2004,** *108* (5), 1537-1543.

(35) Wang, Q.; Wang, W.; Lei, J.; Xu, N.; Gao, F.; Ju, H. Fluorescence Quenching of Carbon Nitride Nanosheet through Its Interaction with DNA for Versatile Fluorescence Sensing. *Anal. Chem.* **2013,** *85* (24), 12182-12188.

(36) Zhu, C.; Zeng, Z.; Li, H.; Li, F.; Fan, C.; Zhang, H. Single-Layer MoS_2-Based Nanoprobes for Homogeneous Detection of Biomolecules. *J. Am. Chem. Soc.* **2013,** *135* (16), 5998-6001.

(37) Acerce, M.; Voiry, D.; Chhowalla, M. Metallic 1T Phase MoS_2 Nanosheets as Supercapacitor Electrode Materials. *Nat. Nanotechnol.* **2015,** *10* (4), 313-318.

Figure 1. Schematic illustration of the exfoliation process of ultrathin metallic and semiconductive MoS_2 nanosheets.

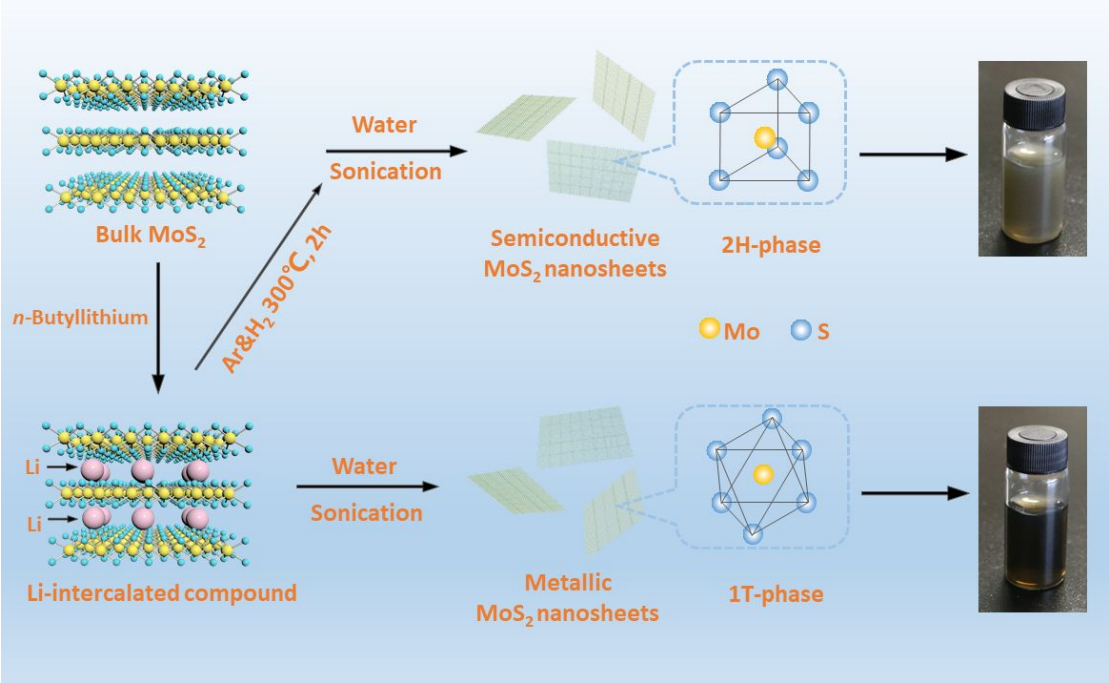

Figure 2. Characterization of ultrathin MoS_2 nanosheets. (a-c) Metallic MoS_2 nanosheets. (d-f) semiconductive MoS_2 nanosheets. (a, d) SEM images. (b, e) TEM images. Inset: (Top) Selected area electron diffraction (SAED) pattern. (Bottom) STEM image. (c, f) AFM images.

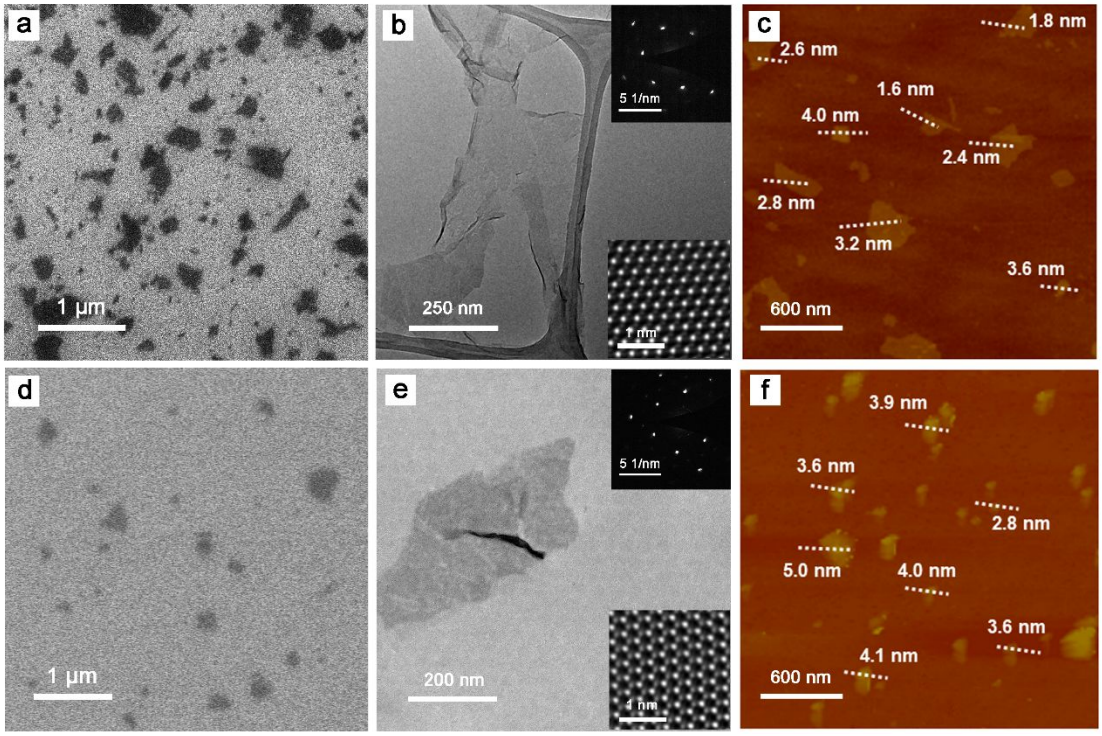

Figure 3. (a) Raman spectroscopy of bulk MoS_2 powder, semiconductive MoS_2 nanosheets, and metallic MoS_2 nanosheets. XPS spectra of Mo 3d mode for (b) metallic MoS_2 nanosheets, (c) semiconductive MoS_2 nanosheets, and (d) bulk MoS_2 powder.

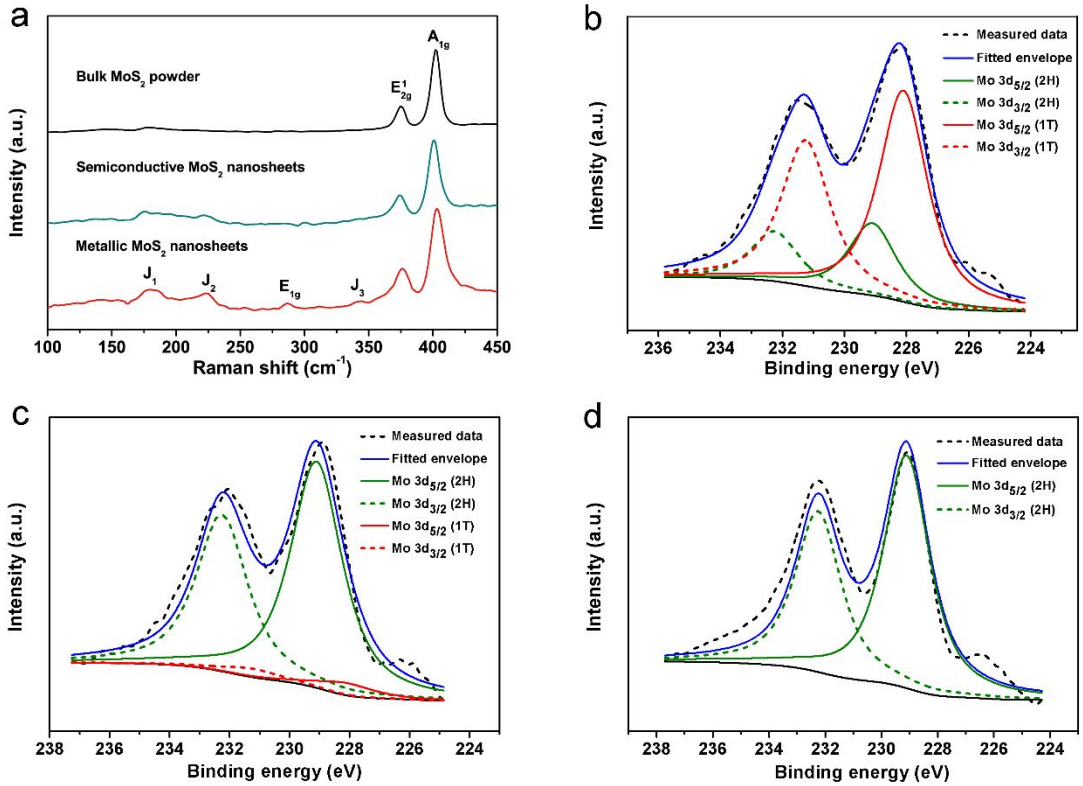

Figure 4. (a) Optical absorption spectrum of metallic and semiconductive MoS_2 nanosheets solution. (b) Comparison of conductivity between metallic and semiconductive MoS_2 nanosheets. Films obtained by (c) metallic and (d) semiconductive MoS_2 nanosheets. Inset: MoS_2 nanosheets solution. (e) The fluorescence intensity of P1 with the same concentration (4.65 μg mL^{-1}) of semiconductive MoS_2 nanosheets and metallic MoS_2 nanosheets. (f) The fluorescence intensity of P1 with 4.65 μg mL^{-1} of metallic MoS_2 nanosheets and 500 μg mL^{-1} of semiconductive MoS_2 nanosheets. The fluorescence spectra was obtained at an excitation wavelength of 490 nm and an emission wavelength range of 505–650 nm. The final concentrations of P1 is 10 nM.

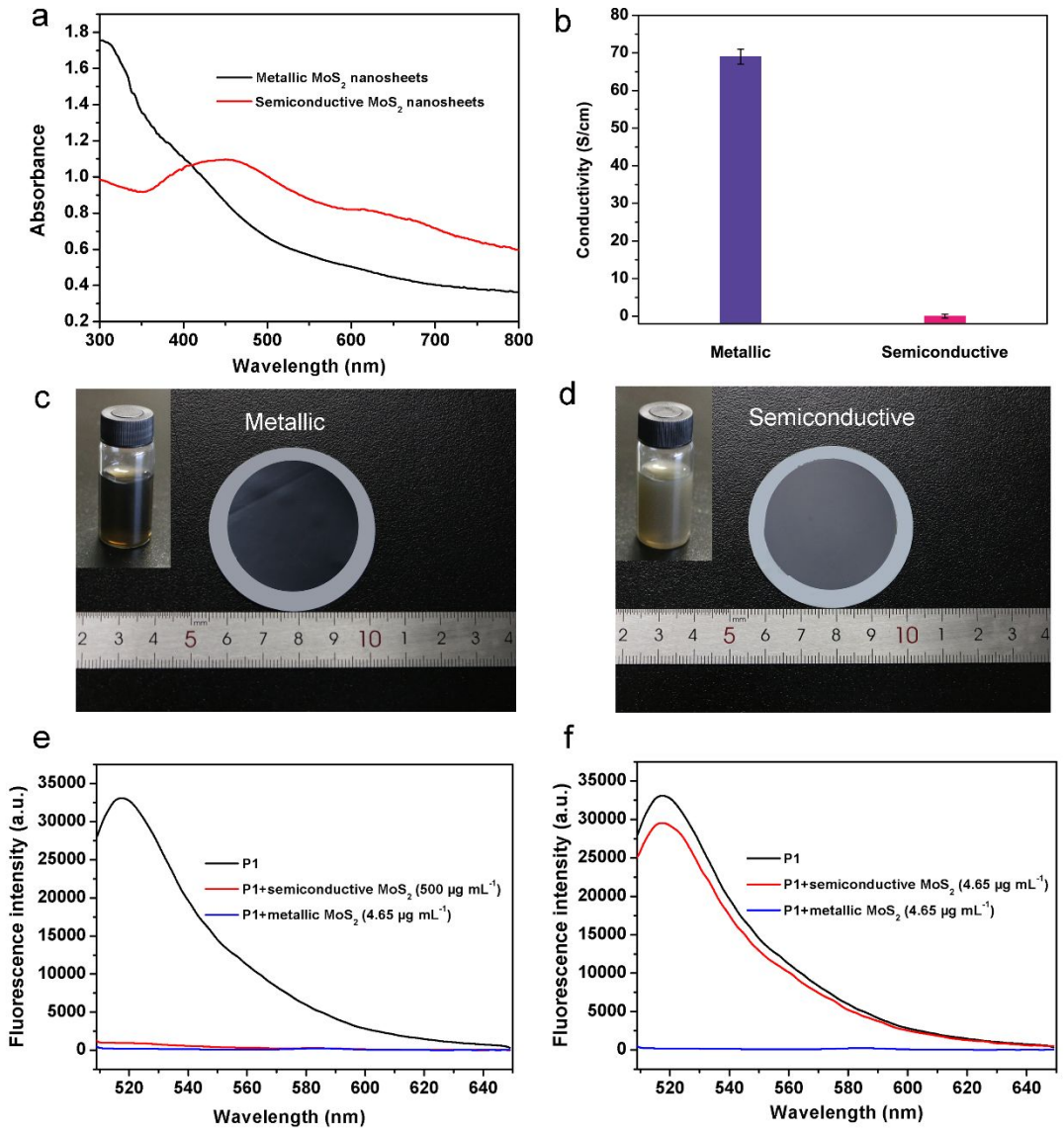

Figure 5. Fluorescence quenching ability of ultrathin metallic MoS_2 nanosheets. (a) Kinetic curves of fluorescence variation of the FAM-labeled probes (10 nM) with different concentrations of MoS_2 nanosheets in 10 min (top to bottom: 0, 0.93, 1.86, 2.79, 3.72, 4.65, 5.58, and 6.51 μg mL^{-1}). (b) Quenching of the probe fluorescence by MoS_2 nanosheets over wavelengths between 505 and 650 nm, excitation at 490 nm. (c) The fluorescence intensity of P1 and P1T1 duplex under various concentrations of MoS_2 nanosheets. The error bars stand for standard deviation of three parallel experiments. (d) The recovery efficiency of MoS_2 nanosheets $(F_0–F)/F_0$ with different concentrations.

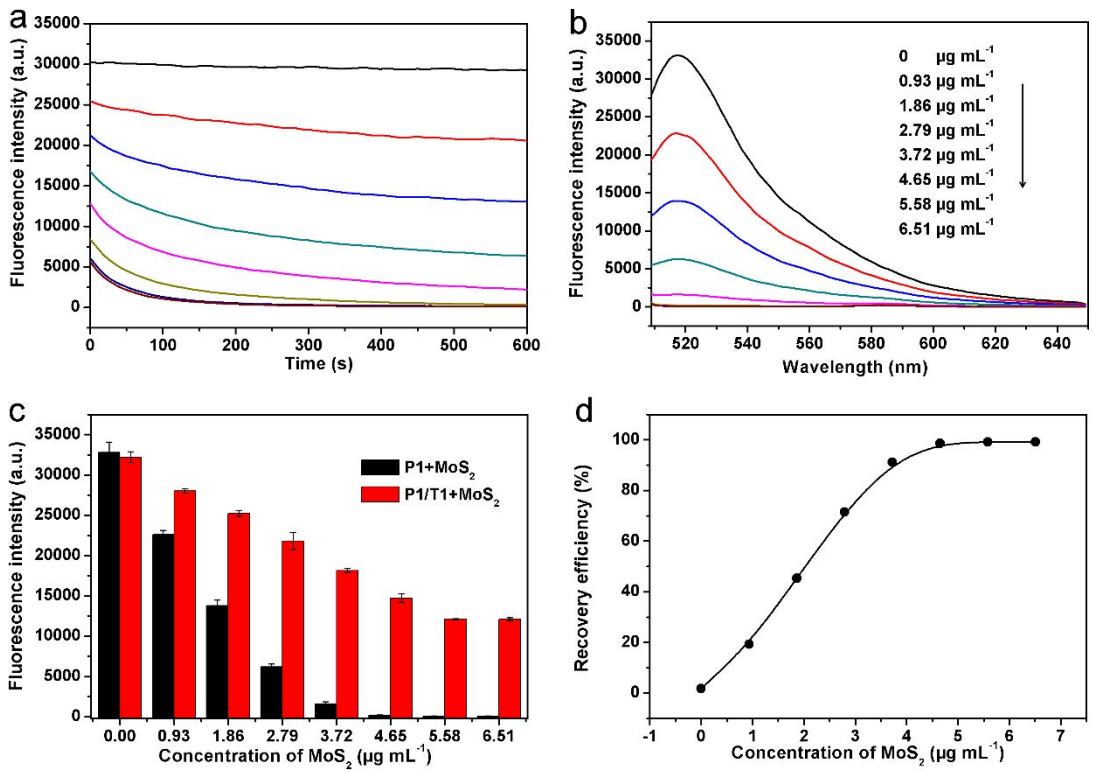

Figure 6. (a) 1T-phase content of metallic MoS_2 nanosheets with various storage times from 1 to 7 days. (b) XPS spectra of Mo 3d mode for metallic MoS_2 nanosheets with various storage times from 1 to 7 days. (c) Fluorescence quenching efficiency of ultrathin metallic MoS_2 nanosheets with various storage times from 1 to 7 days.

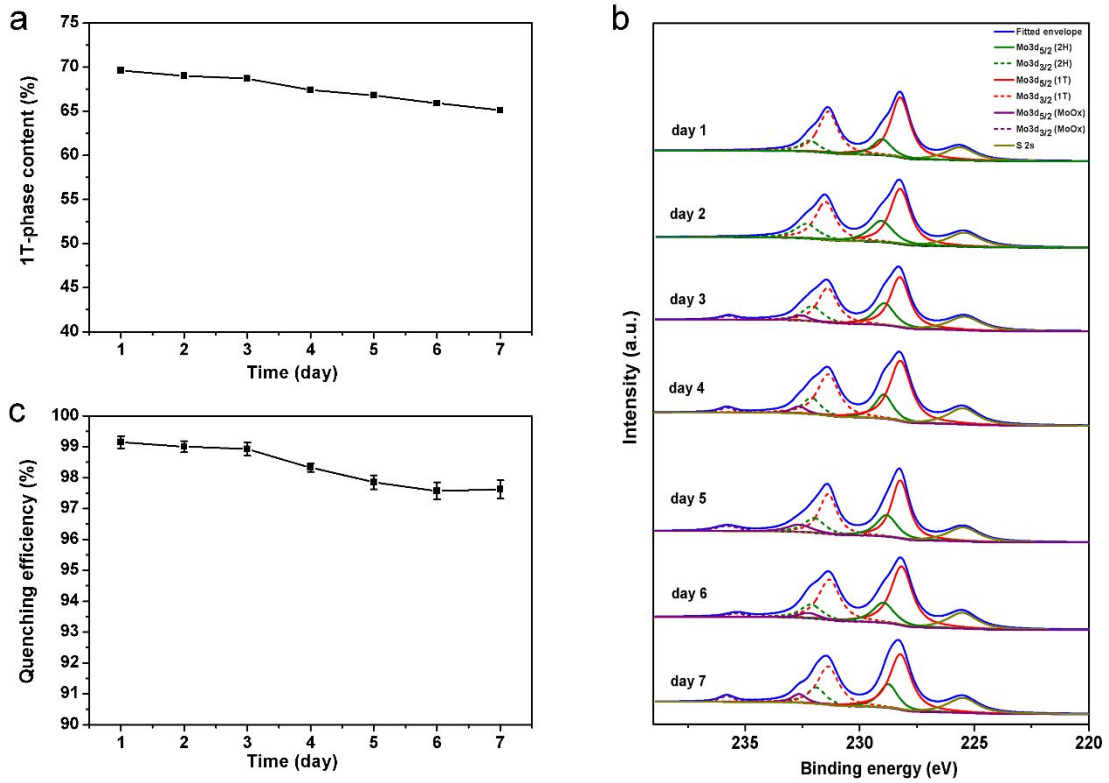

Figure 7. Detection performance of metallic MoS_2 nanosheets. (a) Fluorescence spectra for FAM-labeled P1 (10 nM) under a series of concentrations of T1 (0, 0.1, 0.5, 1, 2, 4, 6, 8, 10, 15, 20, 25, 30, 35, 50, and 75 nM, respectively). (b) Fluorescence intensity versus T1 concentration. Inset: calibration curve for T1 detection. (c) Fluorescence spectra for Texas red-labeled P2 (15 nM) under a series of concentrations of T2 (0, 0.1, 0.5, 1, 2, 4, 6, 8, 10, 15, 20, 25, 30, 35, 50, and 75 nM, respectively). (d) Fluorescence intensity versus T2 concentration. Inset: calibration curve for T2 detection.

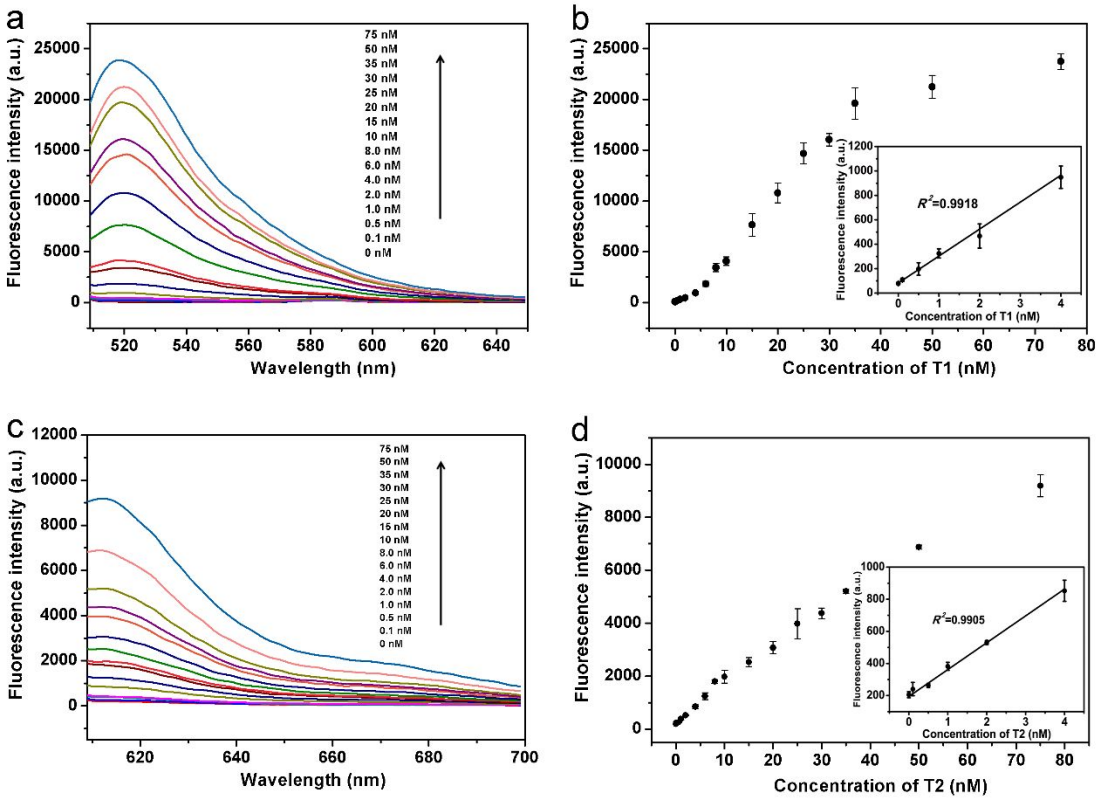

Figure 8. Fluorescence spectra for simultaneous detection of T1 and T2. Two probes P1 and P2 were mixed in the presence of different targets. (a) In the presence of T1. (b) In the presence of T2. (c) In the presence of T1 and T2. (d) In the absence of T1 and T2. The final concentrations are 3 nM of P1/T1 and 10 nM of P2/T2.

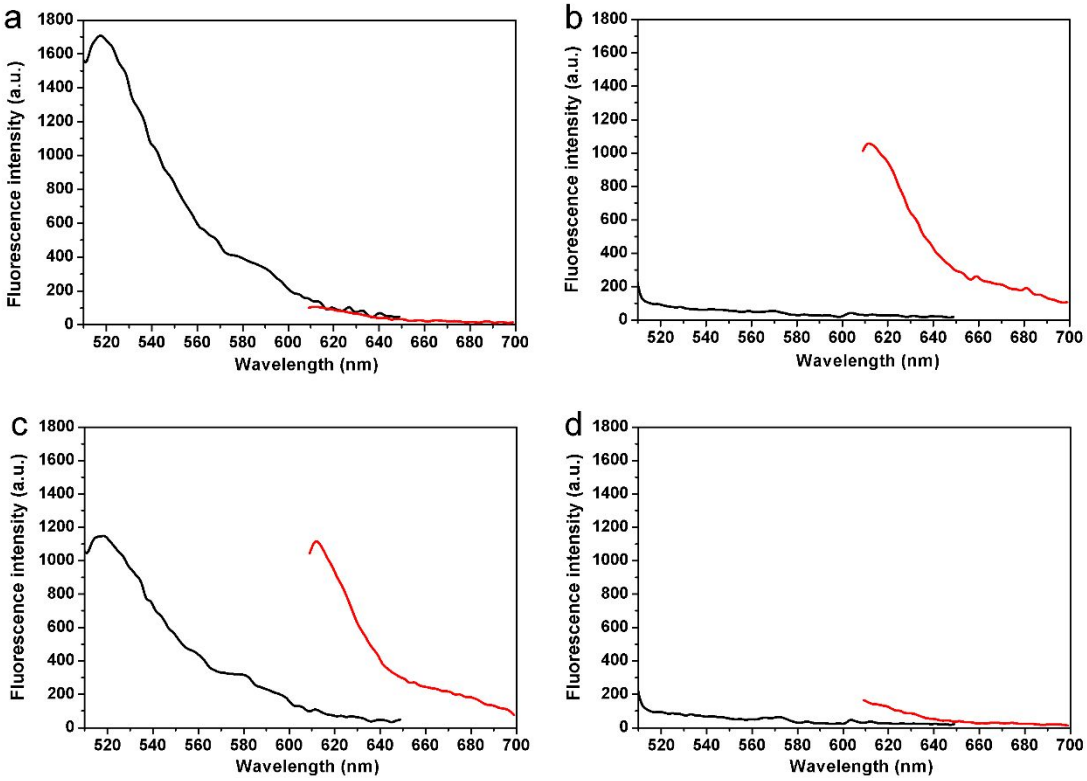

TOC

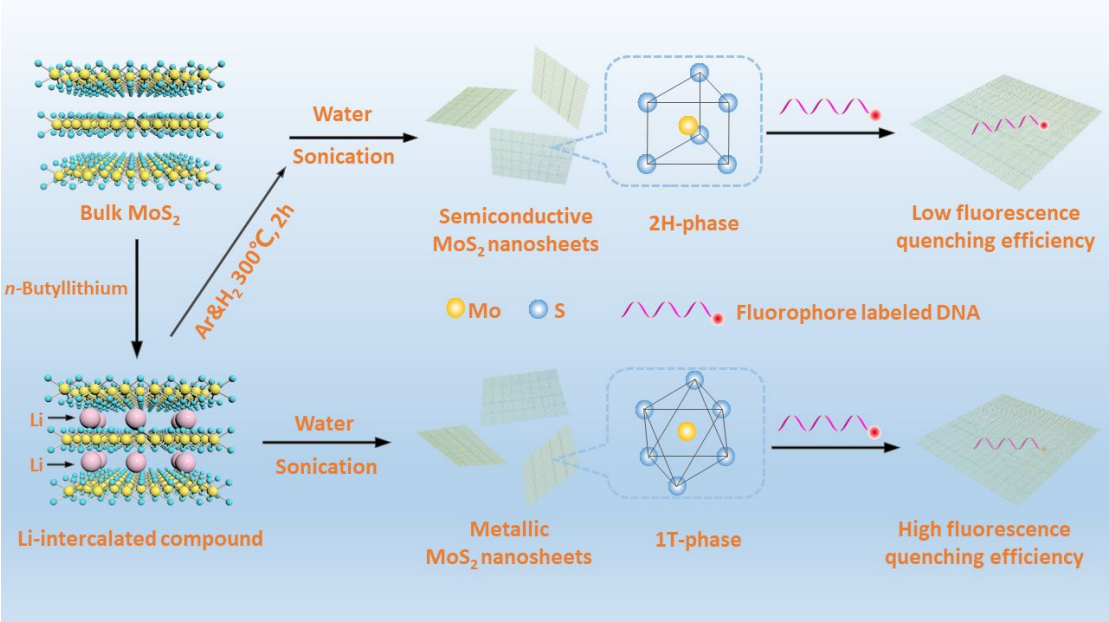
Bulk MoS_2
n-Butyllithium
Ar&H_2 300°C, 2h
Li
Li
Li-intercalated compound
Water
Sonication
Semiconductive MoS_2 nanosheets
2H-phase
Low fluorescence quenching efficiency
Mo
S
Fluorophore labeled DNA
Water
Sonication
Metallic MoS_2 nanosheets
1T-phase
High fluorescence quenching efficiency